Kinematic and dynamic pair collision statistics of sedimenting inertial particles relevant to warm rain initiation

Bogdan Rosa[1], Hossein Parishani[2], Orlando Ayala[2], Lian-Ping Wang[2] & Wojciech W. Grabowski[3]

[1]Institute of Meteorology and Water Management, Poland
[2]Department of Mechanical Engineering, University of Delaware, USA
[3]Mesoscale and Microscale Meteorology Division, National Center for Atmospheric Research,USA

E-mail: bogdan.rosa@imgw.pl

Abstract. In recent years, direct numerical simulation (DNS) approach has become a reliable tool for studying turbulent collision-coalescence of cloud droplets relevant to warm rain development. It has been shown that small-scale turbulent motion can enhance the collision rate of droplets by either enhancing the relative velocity and collision efficiency or by inertia-induced droplet clustering. A hybrid DNS approach incorporating DNS of air turbulence, disturbance flows due to droplets, and droplet equation of motion has been developed to quantify these effects of air turbulence. Due to the computational complexity of the approach, a major challenge is to increase the range of scales or size of the computation domain so that all scales affecting droplet pair statistics are simulated. Here we discuss our on-going work in this direction by improving the parallel scalability of the code, and by studying the effect of large-scale forcing on pair statistics relevant to turbulent collision. New results at higher grid resolutions show a saturation of pair and collision statistics with increasing flow Reynolds number, for given Kolmogorov scales and small droplet sizes. Furthermore, we examine the orientation dependence of pair statistics which reflects an interesting coupling of gravity and droplet clustering.

1. Introduction

Turbulent collision-coalescence of cloud droplets is a necessary and important step for the development of warm rain (Wang *et al.*, 2006; Xue *et al.*, 2008; Wang & Grabowski, 2009). The motivation of our study is to investigate the transformation of cloud droplets of about 10 μm to small rain droplets of 50 to 100 μm in radius. This transformation is mostly governed by gravitational collision-coalescence but it could also be significantly accelerated by air turbulence (Xue *et al.*, 2008). Quantitative understanding of turbulent collision-coalescence of cloud droplets is still incomplete as not all the scales affecting the pairwise interactions of cloud droplets in turbulent air have been fully resolved experimentally or numerically. In recent years, our group has been developing a direct numerical simulation (DNS) tool (Ayala *et al.*, 2007; Rosa & Wang, 2010; Parishani *et al.*, 2010) to quantify the rate of turbulent collision of cloud droplets, both without and with droplet-droplet aerodynamic interactions. Due to the high computational cost and memory requirement, DNS of turbulent collision-coalescence is

limited to small Taylor microscale flow Reynolds numbers ($R_\lambda \approx 100$), or equivalently to a small physical domain size at a given flow dissipation rate in a turbulent cloud. The Reynolds number is defined as $R_\lambda = \sqrt{15}u'^2\tau_k/\nu$ where u' is r.m.s. fluctuation velocity in a given direction, τ_k is Kolmogorov time and ν is fluid viscosity. In this paper, we discuss our efforts in performing DNS at higher grid resolutions in order to examine the flow Reynolds number dependence of kinematic pair collision statistics of cloud droplets. Since most previous studies concern statistics of non-sedimenting inertial particles, we also investigate how the gravity alters the structure (namely the non-isotropic characteristics) and magnitude of pair statistics. In addition, the effect of large-scale forcing scheme on the pair and collision statistics is studied by comparing results from a deterministic forcing with those from a random forcing scheme. These together advance our quantitative understanding of the effect of turbulence on warm rain initiation through droplet growth by turbulent collision-coalescence.

2. Dependence on flow Reynolds number

DNS is a bottom-up approach where turbulent air motion at the dissipation-range scales (mm to cm scales) and a limited range of inertial-subrange scales – currently up to $\mathcal{O}(50$ cm) – are resolved, but larger-scale motion is represented by a forcing scheme. This approach is based on the assumption that pair statistics (i.e., the radial distribution function RDF - a local measure of the preferential concentration of droplets and the relative velocity measured along the line-of-centers) relevant to collision-coalescence are mostly governed by dissipation-range turbulence dynamics since the size and inertial response time of cloud droplets are typically small compared to length and time scale of turbulent motion in the inertial subrange. However, as the droplet size is increased, some inertial subrange scales of fluid motion can also contribute to pair statistics and as such it is desirable to systematically increase the range of flow scales covered in DNS or equivalently the computational domain size.

Recently, we have parallelized our DNS codes using MPI (Message Passing Interface) to enable DNS at higher grid resolutions (256^3 to 512^3) with proportionally larger number of droplets maintaining a realistic cloud liquid water content. Details of the MPI implementation have been reported by Rosa & Wang (2010); Parishani *et al.* (2010); Dmitruk *et al.* (2001). Currently, our MPI implementation is based on domain decomposition in one spatial dimension only. The challenge of the MPI implementation is the concurrent handling of two different representations: an Eulerian grid-based representation of the turbulent flow field and a Lagrangian representation to track the motion and interactions of freely-moving droplets. The MPI code can also treat droplets of several different sizes, allowing some consideration of droplet size distribution (i.e., a polydisperse suspension). At 1024^3 grid resolution, we were able to achieve Taylor microscale Reynolds number of $R_\lambda = 324$ (Rosa *et al.*, 2012), but including droplets at this grid resolution will likely require two-dimensional domain decomposition (*i.e.*, better parallel scalability of the code).

Droplets tracking starts from the moment when the flow becomes statistically stationary. The initial distribution of the droplets is random and spatially uniform. At the beginning the velocity of each droplet is made equal to the local velocity of the background turbulent flow at the droplet location. Equation of motion includes body force, droplet inertia and Stokes drag. Depending on the size of the domain, the relaxation of the droplet system takes about 4 to 5 eddy turnover times. Then kinematic statistics of the droplets are calculated at each time step and then averaged over time at the post-processing stage. For a given droplet size, we study whether and when the dependence of pair and collision statistics on the flow Reynolds number saturates. This provides an indication whether all relevant scales of turbulent motion are considered in DNS, and can be used to guide the development of a theoretical model addressing the effect of flow Reynolds number, similar to the study of RDF for non-sedimenting particles by Collins &

Keswani (2004).

Figure 1 shows monodisperse RDF and radial relative velocity as a function of droplet radius, for different R_λ. These kinematic statistics have been computed neglecting droplet-droplet aerodynamic interactions. Kinematic pair statistics from the low resolution DNS (grid size

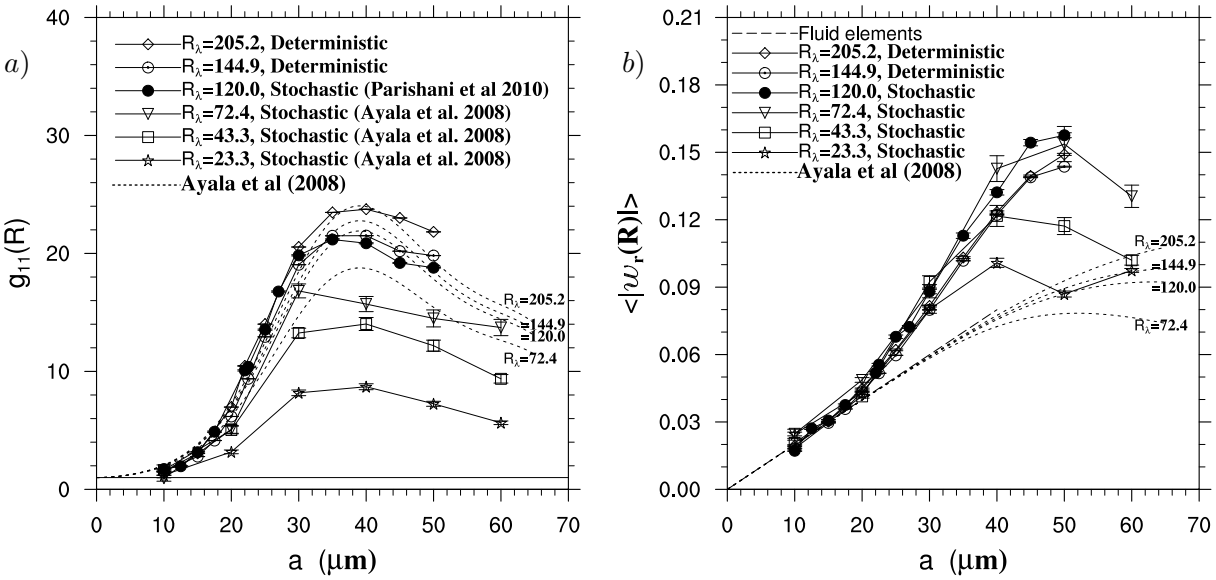

Figure 1. Monodisperse RDF a) and radial relative velocity b) as a function of droplet radius for different R_λ. The dashed lines represent theoretical values calculated from formulas developed by Ayala *et al.* (2008a). All simulations have been performed for energy dissipation $\epsilon = 400$ cm^2/s^3.

from 32^3 to 128^3) were developed in the past using an OpenMP implementation (Ayala *et al.*, 2008b), with a stochastic large-scale forcing. New simulations at higher grid resolutions (256^3 and 512^3) for non-interacting droplets have been performed using our new MPI code. In the new simulations the turbulent flow is driven by a deterministic forcing scheme. Together these data set covers the range of Reynolds numbers from 23.3 to 205.2. Figure 1a shows that the RDF for the larger droplets (greater than 20 μm) increases with increasing flow Reynolds number. At 30 μm, RDF appears to saturate when $R_\lambda > 120$. In other words, the saturation occurs at a higher flow Reynolds number (or larger computational domain size) for larger droplets, consistent with the fact that a wider range of scales affects the pair statistics of larger droplets. Details regarding technical aspects of computation of the RDF are discussed in Wang *et al.* (2000). Radial relative velocities calculated in the same simulations are shown in figure 1b. Again, they appear to saturate and the saturation for larger droplets occurs at a higher R_λ. This observed saturation partially justifies the use of DNS approach at flow Reynolds numbers significantly less than those in real clouds. Also shown in both plots are results of the theoretical prediction developed by Ayala *et al.* (2008a). The difference between the theory and data for radial relative velocity is evident, implying that, for the monodisperse cases, the theory needs to be improved.

3. Analysis of non-isotropic nature of kinematic pair statistics

There have been relatively few DNS studies reporting geometric collision rates of sedimenting inertial particles (Ayala *et al.*, 2008b; Franklin *et al.*, 2005, 2007). In the context of cloud droplets, gravitational sedimentation has to be included. The coupling of gravitational settling

and inertia-induced trajectory bias may cause the pair statistics (i.e. RDF and radial relative velocity) to depend on the orientation of the droplet pair separation vector relative to the vertical direction. Such non-isotropic characteristics are analyzed in our simulations to extend our understanding of pair statistics for sedimenting droplets in order to shed light on how to better parameterize kinematic pair statistics of cloud droplets.

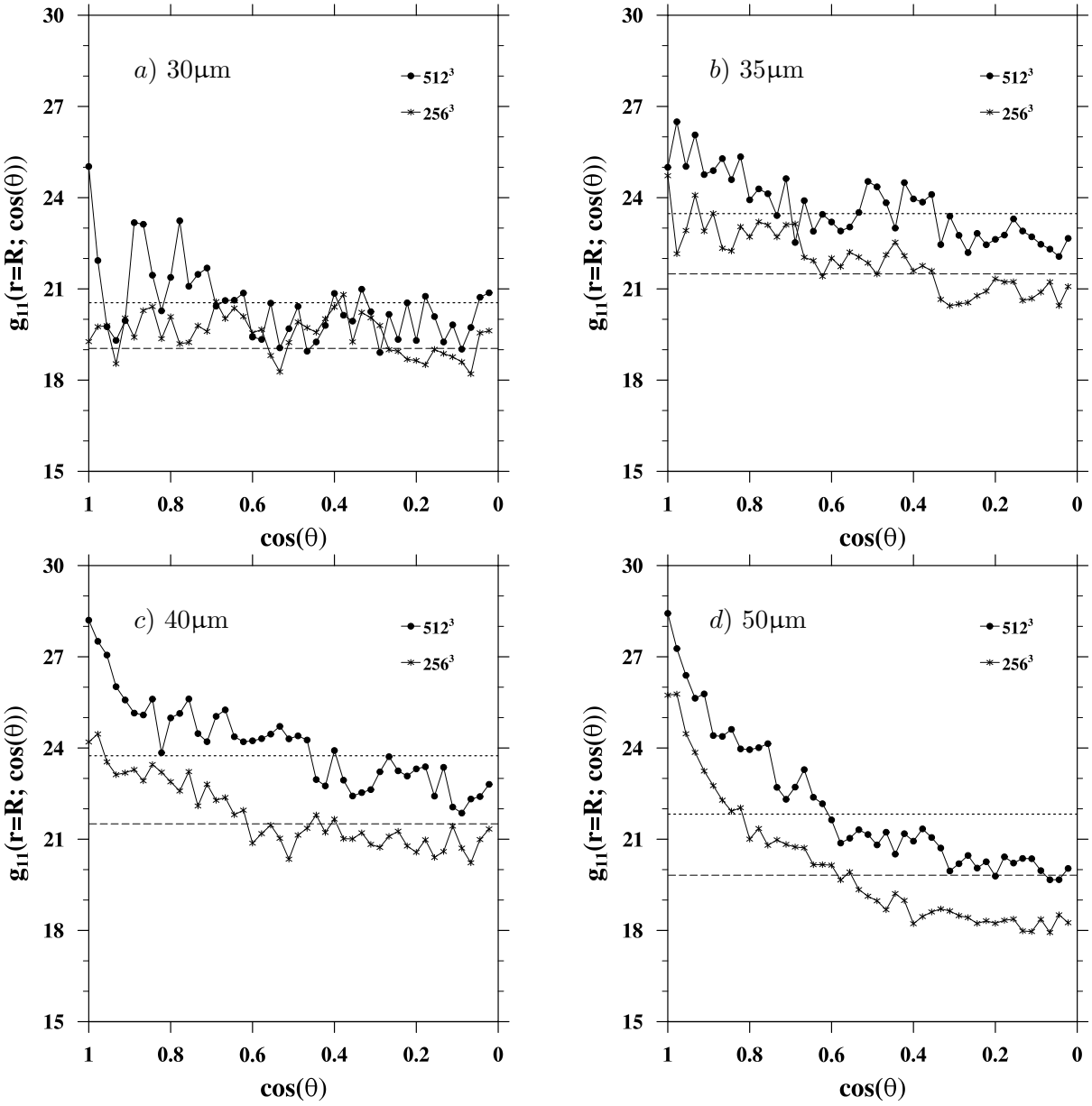

Figure 2. Dependence of monodisperse pair density on the orientation angle as shown by the angle-dependent radial distribution function: (a) 30 μm (b) 35 μm (c) 40 μm (d) 50 μm. Two horizontal lines mark the values of the usual orientation-averaged radial distribution functions performed at 256^3 grid (dash line) and 512^3 grid (dotted line). Droplets are treated as ghost particles. Energy dissipation rate used in the simulations is $\epsilon = 400$ cm^2/s^3.

The DNS data have been obtained from two series of numerical experiments performed at two different grid resolutions (256^3 and 512^3) with an energy dissipation rate of $\epsilon = 400$ cm^2/s^3.

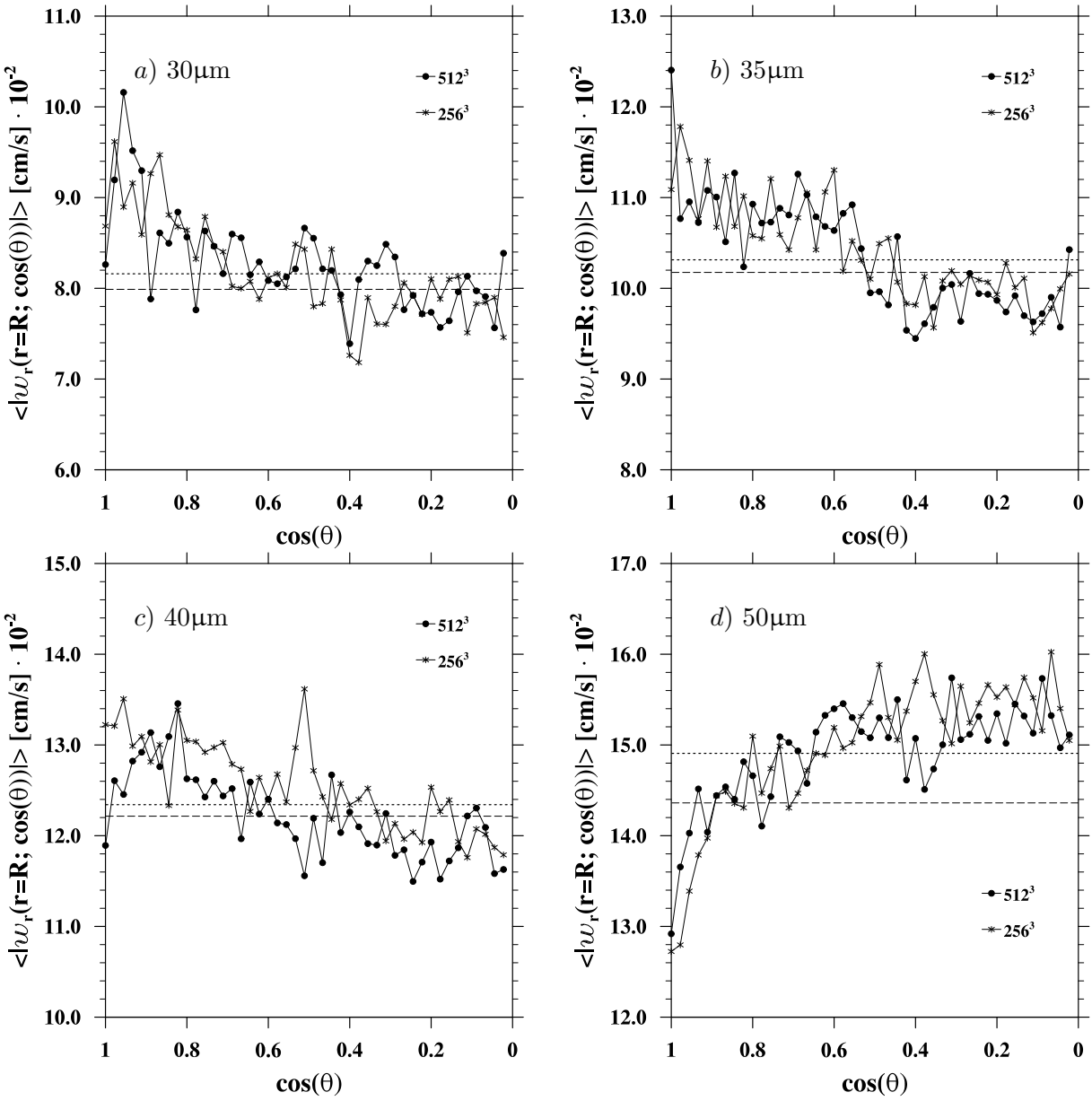

Figure 3. Radial relative velocity of different droplet sizes as a function of the orientation angle. Two horizontal lines indicate the average values of the radial relative velocity corresponding to two simulations performed at 256^3 (dash) and 512^3 (dotted) grid.

For each resolution we simulated motion of non-interacting cloud droplets with radii ranging from 10 to 50 μm. At each run only monodisperse system was considered. Figure 2 shows the pair density of nearly touching droplets, normalized by the mean pair density, as a function of the orientation angle θ. Here we present the results only for the four selected droplet sizes, namely: 30, 35, 40 and 50 μm. Clearly, the local pair density only depends on the polar angle θ. In addition, the droplets of same size are indistinguishable so the pair densities at θ and $\pi - \theta$ are identical. Therefore, the results are shown here only for the range of $0 \leq \theta \leq 90°$. The angle $\theta = 0°$ in figure 2 corresponds to the case in which a line joining the centers of the droplets is parallel to gravity direction. For case in which the droplets are located along a line perpendicular to the gravity θ is equal 90°. The optimal approach for presenting the angle dependence of RDF

is to divide the surface area of the collision sphere into equal bins. The surface area covered from θ to $\theta + d(\theta)$ is $2\pi R^2 \sin(\theta) d(\theta)$ which in turn reduces to $2\pi R^2 d[-\cos(\theta)]$. Therefore, dividing $\cos(\theta)$ equally is equivalent to dividing the surface area of the collision sphere into equal bins. Due to the limited number of samples (pairs) only 45 equal bins have been used.

We can draw several important conclusions from the results shown in figure 2. First, the non-isotropic nature of RDF becomes increasing noticeable for larger droplets, say with radius larger than 35 μm. Secondly, there is no apparent difference in the shape of these radial distribution functions obtained in simulations at two different flow Reynolds numbers. The mean value depends on R_λ, as shown in figure 1. The average value of RDF increases with the droplet radius and reaches a maximum at 40 μm in radius. Figure 2 shows that, for 50 μm droplets, the number of pairs aligned vertically is a factor of 1.4 larger than the number of pairs aligned horizontally. This could be related to the effect of preferential sweeping (Wang & Maxey, 1993) that drives some droplets to move on vertically aligned tracks around a horizontally oriented vortical structures.

A similar approach has been used to illustrate the angle dependence of radial relative velocity for the identical droplet sizes (figure 3). For the same bins the magnitude of radial relative velocity between every pair separated at $r = R$ has been computed and then averaged over time. The angular distribution of the radial relative velocity is different from that observed for the RDF. Even for 25 μm to 30 μm droplets, the anisotropy is present. For droplets smaller than 25 μm, the results contain too large statistical uncertainties to draw a firm conclusion. The average value of the relative velocity increases with the size as more and more scales of turbulent motion contribute to the relative motion. For droplet sizes up to 40 μm the relative velocity is greater for pairs oriented vertically. However, for 50 μm droplets, the trend is different, namely, largest relative velocity is found for pairs aligned horizontally. The exact reason for this change in the angular dependence of relative velocity remains to be understood. In general, the relative differences in velocities depend less on the Reynolds number than it was for RDF.

For a more conclusive analysis, the statistical uncertainties in the data have to be reduced, which can be achieved either by increasing the number of droplets or increasing the simulation time.

4. Effect of large-scale forcing scheme on pair statistics

In order to sustain the turbulent flow in DNS, a continuous input of kinetic energy is provided by a large-scale forcing scheme. The energy from low wave numbers propagates to small turbulent structures until the viscous dissipation acts to remove the kinetic energy according to Kolmogorov's universal equilibrium theory. A balance between the energy input from large-scale forcing and the energy depletion due to the viscous dissipation leads to a statistically stationary turbulent flow. For a limited range of scales covered in DNS, it is not clear whether the nature of large-scale forcing scheme affects the pair and collision statistics of droplets. Qualitatively, this issue is related to the question of the coupling of turbulent motion at small scales with that at large scales, which in turn is related to the question of Reynolds number dependence. Another issue is whether droplet pairs statistics respond to forced large scales directly (due to inertial effects) if the range of scales in DNS is limited. To help address these, we compare here two sets of DNS results obtained based on two different methods of large scale flow forcing: a deterministic scheme akin to (Chen & Shan, 1992) and a stochastic scheme developed by Eswaran & Pope (1988).

In the deterministic forcing, the energy levels of two inner shells ($0.5 < |\mathbf{k}| < 1.5$ and $1.5 < |\mathbf{k}| < 2.5$) corresponding to the largest scales are specified to be $E(1) = 0.55544$ and $E(2) = 0.159843$, respectively. These prescribed values follow the $k^{-5/3}$ energy spectrum taking into account the deviation of the actual number of modes in each shell from the shell volume.

The total number of modes forced at each time step is 80. The velocity field can be initialized to any random field. The algorithm forces the Fourier modes of $|\mathbf{k}| < 2.5$ by amplifying the velocity vectors to yield the above prescribed energy levels.

In the stochastic forcing scheme, a Langevin stochastic model is used. For each mode, six independent random Uhlenbeck-Ornstein processes are combined to specify the Fourier coefficients of a complex vector forcing term (Eswaran & Pope, 1988) in the Fourier space for modes with $|\mathbf{k}| < \sqrt{8}$. Similar to the deterministic forcing, a total number of 80 modes are forced at each time step. Following the notation of Eswaran & Pope (1988), the two key parameters are specified as: $T_f = 0.038$ as forcing time scale and $\sigma^2 = 447.31$ as variance of the random process.

Since forcing schemes affect mainly the large-scale features of turbulence it is expected that some differences in collision and pair statistics may be noticeable for larger droplet sizes. The motion of small droplets is dominated mainly by small vortical structures, which for the both schemes should be similar.

4.1. Flow characteristics

Turbulent flow is simulated by integrating in time the three-dimensional incompressible Navier-Stokes equations. The parameter that controls the stability of the integration is CFL number. Typically, time step size is adjusted to maximize computational efficiency while maintaining the stability of the flow simulation. Another parameter, which ensures that the smallest scales are fully resolved is the resolution parameter $k_{max}\eta$. This parameter has to be greater than 1. Maintaining these constraints in the two simulations with different forcing schemes does not guarantee that the two flows will have the same flow Reynolds number. Deterministic forcing yields a higher R_λ compared to stochastic forcing. In order to keep the two flows dynamically similar, R_λ from both forcing methods are matched by adjusting the numerical fluid viscosity in the deterministic forcing. Obtaining exactly the same value of R_λ will require some trial and error. In this study, for grid resolution at 256^3, after this trial and error procedure, we obtained $R_\lambda = 120.39$ using deterministic forcing and $R_\lambda = 118.46$, with an average of $R_\lambda = 119.42$. The difference in Reynolds number is only $\sim 1.6\%$.

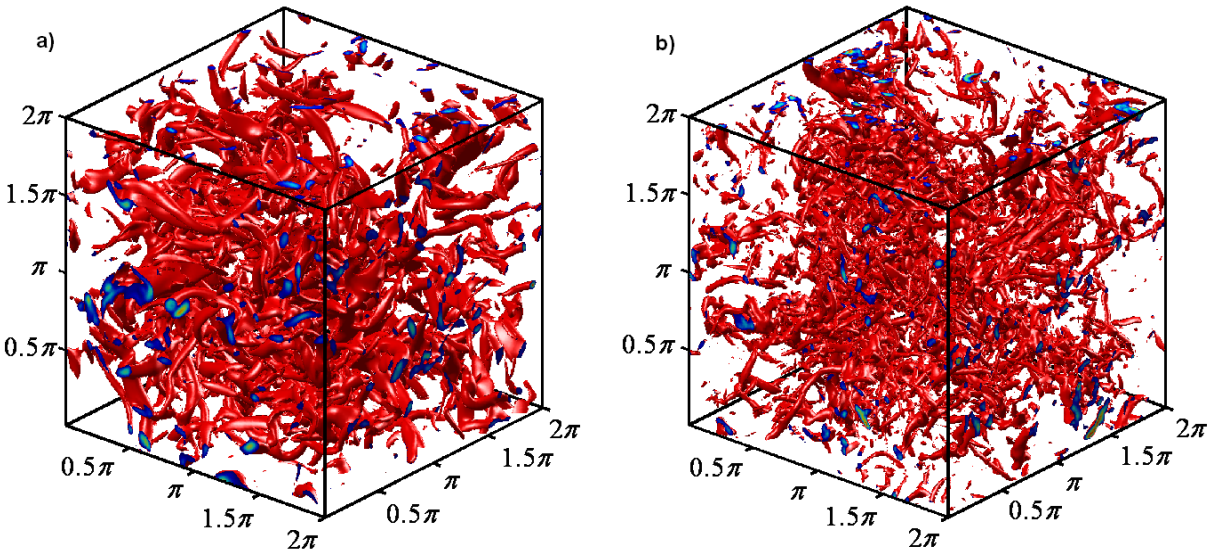

Figure 4. Visualizations of 3D vorticity isosurfaces obtained from *a*) the deterministic forcing scheme and *b*) the stochastic forcing scheme. The contour level is set at twice of the root mean squared value.

Visualizations of vorticity fields at fixed contour level $\omega_c = 2\sqrt{\langle\vec{\omega}^2\rangle}$ (figure 4) lead to the conclusion that the stochastic forcing yields a higher concentration but smaller vortical structures, while the deterministic forcing produces somehow larger and *less random* vortex tubes.

4.2. Collision statistics

Examination of pair statistics of cloud droplets is restricted to sizes ranging from 10 to 50 μm. This range of droplet radii is of the high interest to warm rain initiation. This corresponds to a range of Stokes number $0.06 < St < 1.58$ when the energy dissipation rate is set to 400 $\mathrm{cm}^2/\mathrm{s}^3$. In this study the numerical experiments are limited to self-collision (collision of the same-size droplets). Furthermore, in the simulations, droplets are allowed to reach statistically stationary state in turbulence by running the simulation for about five eddy turnover times before collecting collision statistics. To quantify droplet collision statistics, both RDF and radial relative velocity are studied. For smaller droplet radii (mainly, 10 and 15 μm), significant statistical uncertainties are present in RDF at near-collision separation distances, which can be avoided by using significantly longer time intervals or more droplets. For these cases, we used 60% longer run times compared to that of large-size droplets. The higher uncertainties for small droplets are inherently related to the lower collision rate, making it much harder to obtain reliable statistics for small droplets when compared to large droplets.

RDF of droplets at contact is plotted in figure 5a. It is observed that for small droplets (radii smaller than 20 μm) the RDF is the same no matter which forcing scheme is used. For particles larger than 22 μm ($St > 0.3069$) the difference in RDF tends to grow with droplet size. For example in the simulations at grid size 256^3 and droplet radii 50 μm the deterministic forcing produces 24% higher RDF than the stochastic forcing.

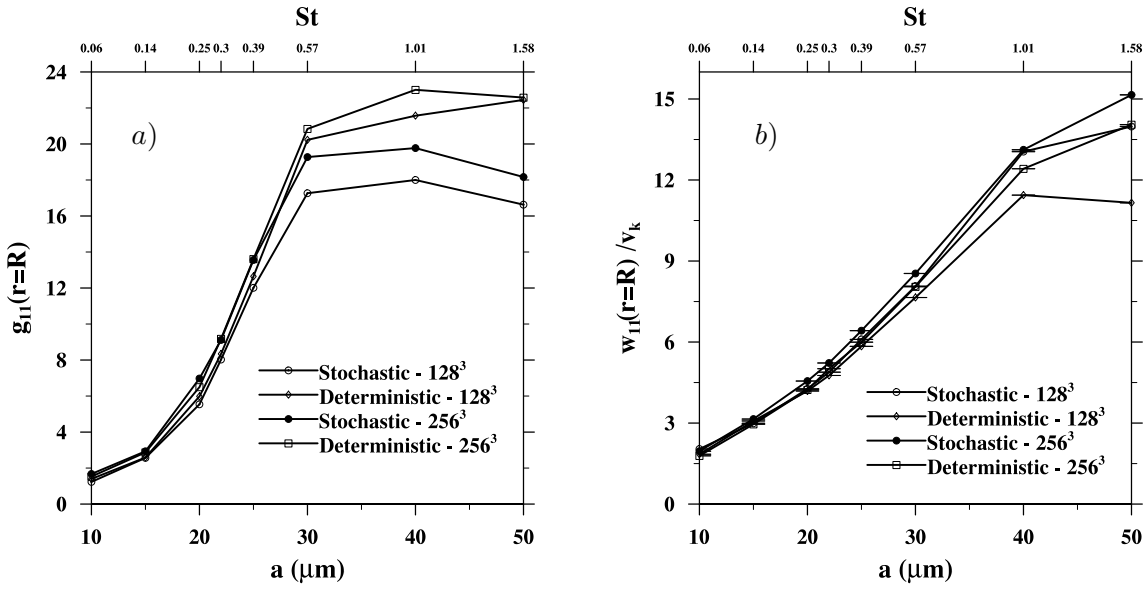

Figure 5. RDF (a) and radial relative velocity (b) at contact as a function of droplet radius, for two grid resolutions and two forcing schemes. Statistics are presented as a function of droplet radius (lower scale) and the Stokes number (upper scale).

Next, radial relative velocity between droplets pairs has been computed and then averaged over time to obtain $w_{11}(r = R)$. It is observed (figure 5b) that the forcing method have no effect on the relative velocity of smaller particles while significantly affecting that of droplets larger

than 22 μm. For instance, in results of simulation at 256^3 grid resolution, we observed that the stochastic forcing of flow yields a 25% higher radial relative velocity than the deterministic method (for 50 μm droplets at contact). As expected, the stochastic forcing introduces random motions to the flow and consequently increases fluctuations in droplet velocity which in turn leads to higher relative velocity for droplets.

To conclude, we find that the pair statistics of smaller droplets (or small Stokes numbers) are insensitive to the nature of large-scale forcing scheme, while for larger droplets they depend on the forcing scheme. The differences also increase with the droplet size. Since the collision kernel is the product of RDF and radial relative velocity, the effect of forcing on RDF and the effect on relative velocity almost cancel each other out, making the collision kernel very insensitive to the large-scale forcing.

5. Conclusions

In this paper, we reported our recent efforts in increasing the scalability of our hybrid DNS codes for simulating turbulent collision-coalescence of cloud droplets. We have implemented MPI based on 1D domain decomposition, making it possible to simulate droplet collision and pair statistics at 256^3 and 512^3 grid resolutions. Further improvement in scalability is being developed by introducing 2D domain decomposition.

Using the 1D domain-decomposition hybrid DNS code, here we examined three important aspects of the DNS concerning turbulent collision-coalescence of cloud droplets. First, we showed that the RDF and the radial relative velocity will reach their saturated values, if all relevant scales of fluid motion are included in the flow simulation. This supports a fundamental assumption in the DNS, namely, DNS at much lower flow Reynolds numbers compared to those in real clouds can be used to quantity turbulent collision-coalescence of cloud droplets. Then we analyzed the non-isotropic nature of kinematic pair statistics. Results show that the effect of non-isotropy in RDF is noticeable only for large cloud droplets with radius greater than 35 μm. There is no apparent difference in the shape of the RDF computed in simulations with different flow Reynolds numbers. The angular dependence of radial relative velocity exhibits different characteristics from those of RDF. Finally, we studied the effect of large-scale forcing on the self-collision statistics of droplets. We found that the deterministic forcing leads to higher accumulation of droplets but smaller radial relative velocity. The collision kernel, which is a product of RDF and radial relative velocity, is then much less sensitive to the large-scale forcing. A finite effect of large-scale forcing is present for larger droplet sizes due to a limited range of scales resolved in DNS.

6. Acknowledgments

This work was supported by the National Science Foundation (NSF) under grants ATM-0527140, ATM-0730766, OCI-0904534, and CRI-0958512. Computing resources are provided by National Center for Atmospheric Research (NCAR CISL-35751010, CISL-35751014, and CISL-35751015).

References

Ayala, 0., Rosa, B. & Wang, L-P. 2008*a* Effects of turbulence on the geometric collision rate of sedimenting droplets. Part 2. Theory and parametrization. *New J. Physics* **10** (075016).

Ayala, 0., Wang, L-P. & Grabowski, W.W. 2007 A hybrid approach for simulating turbulent collision of hydrodynamically-interacting particles. *J. Comp. Phys.* **222**, 51–73.

Ayala, O., Rosa, B., Wang, L. P. & Grabowski, W. W. 2008*b* Effects of turbulence on the geometric collision rate of sedimenting droplets. Part 1. Results from direct numerical simulation. *New Journal of Physics* **10**.

Chen, S. & Shan, X. 1992 High resolution turbulent simulations using the connection machine-2. *Comp. Phys.* **6**, 643–646.

Collins, L. R. & Keswani, A. 2004 Reynolds number scaling of particle clustering in turbulent aerosols. *New Journal of Physics* **6**.

Dmitruk, P., Wang, L. P., Matthaeus, W. H., Zhang, R. & Seckel, D. 2001 Scalable parallel FFT for spectral simulations on a Beowulf cluster. *Parallel Computing* **27** (14), 1921–1936.

Eswaran, E. & Pope, S.B. 1988 An examination of forcing in direct numerical simulations of turbulence. *Computer and Fluids* **16**, 257–278.

Franklin, C. N., Vaillancourt, P. A. & Yau, M. K. 2007 Statistics and parameterizations of the effect of turbulence on the geometric collision kernel of cloud droplets. *Journal of the Atmospheric Sciences* **64** (3), 938–954.

Franklin, C. N., Vaillancourt, P. A., Yau, M. K. & Bartello, P. 2005 Collision rates of cloud droplets in turbulent flow. *Journal of the Atmospheric Sciences* **62** (7), 2451–2466.

Parishani, H., Rosa, B., Grabowski, W.W. & L.-P., Wang 2010 Towards high-resolution simulation of turbulent collision of cloud droplets. *Proceedings of the 7th International Conference on Multiphase Flow, Tampa, Fl, USA* .

Rosa, B., Parishani, H., Ayala, O., Wang, L.-P. & Grabowski, W.W. 2012 High-resolution simulation of turbulent collision of cloud droplets. In *Submitted to Parallel Processing and Applied Mathematics*. Springer.

Rosa, B. & Wang, L.-P. 2010 Parallel implementation of particle tracking and collision in a turbulent flow. In *Parallel Processing and Applied Mathematics* (ed. R. Wyrzykowski, J. Dongarra, K. Karczewski & J. Wasniewski), *Lecture Notes in Computer Science*, vol. 6068, pp. 388–397. Springer.

Wang, L-P. & Grabowski, W.W. 2009 The role of air turbulence in warm rain initiation. *Atmospheric Science Letters* **10**, 1–8.

Wang, L-P. & Maxey, M.R. 1993 Settling velocity and concentration distribution of heavy particles in a forced isotropic and homogeneous turbulence. *J. Fluid Mech.* **256**, 27–68.

Wang, L.-P., Wexler, A. & Zhou, Y 2000 Statistical mechanical description and modelling of turbulent collision of inertial particles. *J. Fluid Mech.* **415**, 117–153.

Wang, L-P., Xue, Y., Ayala, 0. & Grabowski, W.W. 2006 Effects of stochastic coalescence and air turbulence on the size distribution of cloud droplets. *Atmospheric Research* **82**, 416–432.

Xue, Y., Wang, L-P. & Grabowski, W.W. 2008 Growth of cloud droplets by turbulent collision-coalescence. *J. Atmos. Sci.* **65**, 331–356.